Chinese Chemical Letters 33 (2022) 2630–2634

Contents lists available at ScienceDirect

Chinese Chemical Letters

journal homepage: www.elsevier.com/locate/cclet

A unique organic-inorganic hybrid Fe^{III}–Pr^{III}-included 2-germano-20-tungstate and its electrochemical biosensing properties

Xiaoyi Liu[1], Limin Cui[1], Jun Jiang, Fan Ji*, Junwei Zhao*

College of Chemistry and Chemical Engineering, Henan University, Kaifeng 475004, China

ARTICLE INFO

Article history:
Received 25 August 2021
Revised 16 September 2021
Accepted 23 September 2021
Available online 30 September 2021

Keywords:
Polyoxometalate
Germanotungstate
Heterometallic polyoxotungstate
Electrochemistry
Biosensing

ABSTRACT

An organic-inorganic hybrid Fe^{III}–Pr^{III}-included 2-germano-20-tungstate $[Pr(H_2O)_8]_2H_2[Fe_4(H_2O)_4(pca)_4Ge_2W_{20}O_{72}]\cdot 34H_2O$ (Hpca = 2-pyridinecarboxylic acid) (1) was hydrothermally prepared. Its polyoxoanion comprises one tetra-Fe^{III} incorporated $[Fe_4(H_2O)_4(pca)_4Ge_2W_{20}O_{72}]^{8-}$ hybrid entity and two $[Pr(H_2O)_8]^{3+}$ ornamental cations. The $[Fe_4(H_2O)_4(pca)_4Ge_2W_{20}O_{72}]^{8-}$ 2-germano-20-tungstate entity can be regarded as an infrequent *S*-type $[Ge_2W_{20}O_{72}]^{16-}$ cluster pocketed by four $[Fe(H_2O)(pca)]^{2+}$ cations. The *S*-type $[Ge_2W_{20}O_{72}]^{16-}$ cluster could be imagined as condensation of two divacant Keggin $[\alpha\text{-}GeW_{10}O_{37}]^{10-}$ segments by sharing two atoms. It is of interest is that carboxyl O and pyridine N atoms on pca ligands concurrently bind with Fe^{3+} cations in a five-membered heterocyclic fashion to increase the stability of the whole structure. Furthermore, the electrochemical biosensing properties of 1 as the modified electrode material have been investigated for detecting norepinephrine (NPP), showing a low detection limit of 3.25 μmol/L. This work not only enriches structures of heterometallic germanotungstates (GTs), but also expands applications of polyoxometalates (POMs) in the electrochemical biosensing field.

POMs are an outstanding class of metal-oxygen anionic clusters composed of high-oxidation-state early transition metals (including Mo^{VI}, W^{VI}, V^{V}, Nb^{V}, Ta^{V}) with structural diversities and glamorous topological aesthetics, which have been widely used in various fields, such as medicine, optics, catalysis, material science and electronic sensors [1–11]. Lacunary POMs can be considered as one extraordinary kind of inorganic multidentate ligands for integrating transition-metal (TM) or rare-earth (RE) cations to produce diverse TM or RE-encapsulated POMs with fascinating architectures and newfangled properties [12–14]. Amongst them, TM-encapsulated POMs possess diversiform metal centers and present possible applications in catalysis, magnetism and electroconductivity [15–19]. For RE-encapsulated POMs, abundant electronic energy levels and flexible coordination modes of RE ions render them to become prospective linkers of lacunary POMs, presenting potential applications in luminescence and catalysis [20–22]. While, the design and preparation of TM-RE-included POMs (TRIPs) have attracted comprehensively growing attention on account of abundant structure types and spacious applications combined with the advantages of these two kinds of metals [23,24]. Even so, continuous explorations on TRIPs still remain less developed because of unavoidable competing reaction amongst TM, RE and POM components [25]. Therefore, the preparation and exploration of TRIPs will remain a long-term and abiding challenge.

GTs, as a significant branch of POMs, have gradually become an attractive research hotspot and a challengeable field displaying latent performances in catalysis, magnetism, materials science and optics [26,27]. Importantly, highly nucleophilic lacunary GTs are generally used as reactants to grasp TM and RE cations to further generate TM–RE-included GTs (TRIGs) [28]. For example, in 2010, a novel Ce–Mn co-embedded GT was prepared by incorporating Ce^{IV} ions into $[Mn_4(H_2O)_2(B\text{-}\alpha\text{-}GeW_9O_{34})_2]^{12-}$, which represents the first case of heterometallic 3d–4f Weakley-type structure [29]. Zhao *et al.* introduced the $\{Ce^{IV}/Mn^{II}/ox^{2-}\}$ system into the trivacant $[\alpha\text{-}GeW_9O_{34}]^{10-}$ precursor to synthesize a neoteric TRIG $[Ce_2(ox)_3(H_2O)_2]_2\{[Mn(H_2O)_3]_2[Mn_4(GeW_9O_{34})_2(H_2O)_2]^{8-}$ (ox = oxalate), which is the first 3-D organic-inorganic hybrid framework assembled from tetra-Mn sandwiched GTs and mixed Mn and Ce connectors [30]. Besides, a heterometallic hexameric GT $[Fe_6Sm_6(H_2O)_{12}(\alpha\text{-}GeW_{10}O_{38})_6]^{23-}$ is composed of divacant $[\alpha\text{-}GeW_{10}O_{38}]^{12-}$ fragments and six $\{Fe\text{-}(\mu_3\text{-}O)_3\text{-}Sm\}$ linkers [31]. Zheng *et al.* reported unprecedented decameric TRIGs $[RE_{29}Ge_{10}W_{106}O_{406}(OH)_4(H_2O)_{28}]^{59-}$ (RE = La^{III}, Ce^{II}) [32]. Our group has also made some progresses on TRIGs such as

---

* Corresponding authors.
E-mail addresses: jifan@henu.edu.cn (F. Ji), zhaojunwei@henu.edu.cn (J. Zhao).

[1] These authors contributed equally to this work.

https://doi.org/10.1016/j.cclet.2021.09.078

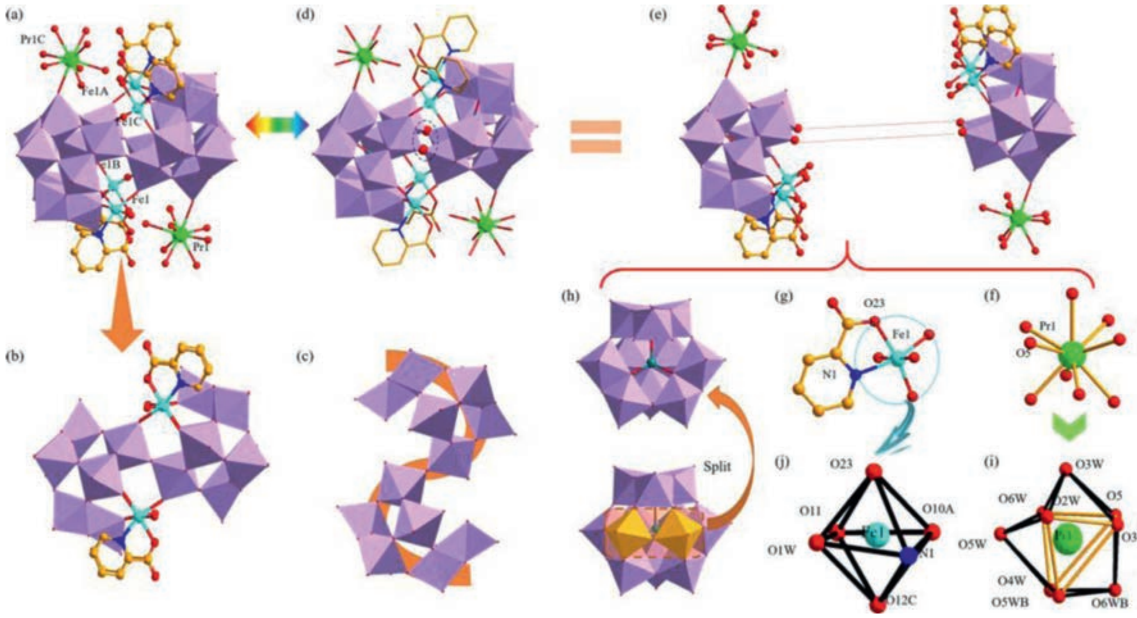

Fig. 1. (a) The **1a** hybrid anion. (b) The $[Fe_4(H_2O)_4(pca)_4Ge_2W_{20}O_{72}]^{8-}$ entity. (c) The *S*-type $[Ge_2W_{20}O_{72}]^{16-}$ cluster. (d) Double oxygen-bridging mode in **1a** anion. (e) Two identical $[Pr(H_2O)_8][Fe_2(H_2O)_2(pca)_2GeW_{10}O_{36}]^-$ moieties. (f) The $[Pr1(H_2O)_8]^{3+}$ cation. (g) The $[Fe1(H_2O)(pca)]^{2+}$ cation. (h) The divacant $[\alpha\text{-}GeW_{10}O_{37}]^{10-}$ segment. (i) The coordination geometry of the $[Pr1(H_2O)_8]^{3+}$ cation. (j) The coordination geometry of the $[Fe1(H_2O)(pca)]^{2+}$ cation. Color distribution: *O*, red; Ge, teal; Pr, bright green; Fe, turquoise; *N*, blue; *C*, light orange; $\{WO_6\}$, lavender. Symmetrical codes: A *-x*, *-y*, 1-*z*; B *x*, *-y*, *z*; C *-x*, *y*, 1-*z*.

tetrameric and 1D Cu-RE encapsulated TRIGs constructed from two $[Cu(en)_2]^{2+}$ or $[Cu(dap)_2]^{2+}$ linkers and $[RE(\alpha\text{-}GeW_{11}O_{39})_2]^{13-}$ (RE = Gd^{III}, Y^{II}) subunits [33–35].

Albeit enormous efforts have been devoted to explore fascinating TRIGs, some challenges still exist due to the following three reasons: (i) The majority of TM ions in TRIGs are Cu^{2+}ions, in contrast, reports on other TM ions are relatively infrequent [29–35]; (ii) Organic ligands of TRIGs are mainly flexible ligands, however, rigid organic ligands were less introduced in the construction of TRIGs [30–35]; (iii) Most of TRIGs are based on monovacant and trivacant fragments, but TRIGs based on divacant fragments or novel building blocks are very scarce [32]. Recently, upon our persistent exploration, using rigid 2-pyridinecarboxylic acid (Hpca), Fe^{3+} and Pr^{3+} cations are simultaneously introduced into the GT system to generate a glamorous pca-functionalized Fe^{III}–Pr^{III}-included 2-germano-20-tungstate $[Pr(H_2O)_8]_2H_2[Fe_4(H_2O)_4(pca)_4Ge_2W_{20}O_{72}]\cdot 34H_2O$ **(1)** including a novel *S*-type $[Ge_2W_{20}O_{72}]^{16-}$ cluster. To our knowledge, such 2-picolinate modified Fe^{III}–Pr^{III} co-embedded GT is very rare. In addition, the *S*-type $[Ge_2W_{20}O_{72}]^{16-}$ cluster is a rarely seen POM segment. Moreover, the solid-state electrochemical properties of **1** have been carried out by entrapping it into a carbon paste electrode (CPE) for detecting norepinephrine (NPP).

The powder X-ray diffraction (PXRD) (Fig. S1 in Supporting information) exhibits that the sample of **1** is pure. Crystallographic data of **1** are provided in Table S1 (Supporting information), showing that **1** belongs to the monoclinic space group *C*2/*m*. The molecular structure of **1** contains a tetra-Fe^{III} incorporated $[Pr(H_2O)_8]_2[Fe_4(H_2O)_4(pca)_4Ge_2W_{20}O_{72}]^{2-}$ **(1a)** hybrid anion with two pendant $[Pr(H_2O)_8]^{3+}$ cations (Fig. 1a). On one hand, the **1a** hybrid anion can be taken as one $[Fe_4(H_2O)_4(pca)_4Ge_2W_{20}O_{72}]^{8-}$ entity (Fig. 1b) suspended by two $[Pr(H_2O)_8]^{3+}$ cations. The tetra-Fe^{III} incorporated $[Fe_4(H_2O)_4(pca)_4\ Ge_2W_{20}O_{72}]^{8-}$ entity is made up of a novel *S*-type $[Ge_2W_{20}O_{72}]^{16-}$ cluster (Fig. 1c) that is stabilized by four $[Fe(H_2O)(pca)]^{2+}$ groups. On the other hand, the **1a** hybrid anion could be also regarded as condensation of two identical $[Pr(H_2O)_8][Fe_2(H_2O)_2(pca)_2GeW_{10}O_{36}]^-$ moieties by sharing O1 and O1A atoms (Fig. 1d). Importantly, in each $[Pr(H_2O)_8][Fe_2(H_2O)_2(pca)_2GeW_{10}O_{36}]^-$ moiety (Fig. 1e), the $[Pr(H_2O)_8]^{3+}$ cation (Fig. 1f) is located at the vertex of $[\alpha\text{-}GeW_{10}O_{37}]^{10-}$ subunit whereas two $[Fe(H_2O)(pca)]^{2+}$ groups (Fig. 1g) are located at the divacant sites of $[\alpha\text{-}GeW_{10}O_{37}]^{10-}$ subunit (Fig. 1h). From the viewpoint of crystallography, only one crystallographically independent Pr^{3+} ion and one crystallographically unique Fe^{3+} ion exist in the crystal structure. The coordination sphere of the $Pr1^{3+}$ cation displays a nine-coordinate twisted tricapped triangular prism (Fig. 1i), in which the O5 atom is from the $[\alpha\text{-}GeW_{10}O_{37}]^{10-}$ segment [Pr–O5: 2.532(16) Å] and the remaining eight oxygen atoms originate from water ligands [Pr-O: 2.464(13)–2.60(2) Å]. In the $Pr1^{3+}$ tricapped triangular prism, the O2W–O6W–O5–O3WB, O5–O3WB–O5WB–O4W and O5WB–O4W–O6W–O2W groups build the three side surfaces of the triangular prism while O3W, O6WB and O5W atoms are respectively located on three capped sites of the tricapped triangular prism. Besides, every $Fe1^{3+}$ cation coordinates to one pca ligand, and every pca ligand adopts the bidentate coordination and coordinates to the $Fe1^{3+}$ cation by means of the O23 and N1 atoms in a five-membered heterocyclic mode (Fig. 1g). The coordination sphere of the $Fe1^{3+}$ cation presents a six-coordinate octahedron (Fig. 1j), in which the O23 and N1 atoms [Fe1–O23: 2.046(11) Å, Fe1–N1: 2.153(12) Å] originate from pca ligand, O12 and O10 atoms [Fe1-O12C: 1.922(10) Å, Fe1–O10A: 1.923(10) Å] come from one $[\alpha\text{-}GeW_{10}O_{37}]^{10-}$ segment and the O11 atom [Fe1–O11: 1.984(10) Å] is from the other $[\alpha\text{-}GeW_{10}O_{37}]^{10-}$ segment.

Ulteriorly, the 3D stacking arrangements of **1a** hybrid anions along the *a*, *b* and *c* axes are exhibited in Fig. 2. **1a** hybrid anions show the similar –ABAB– arrangement pattern in the *bc*, *ac* and *ab* planes (Figs. 2a–c). Simplified views of anions of 1 are shown in Figs. 2d–f. Interestingly, compared to the *bc* and *ac* planes, adjacent A and B layers viewed along the *c* axis are aligned in a staggered fashion, which contributes to decreasing the steric hindrance as much as possible.

NPP is a neurotransmitter and belongs to catecholamines in chemical structure. It is recommended as a vasopressor of first choice for clinical and pharmacological purposes, but this high dose catecholamine therapy may cause myocardial infarction, im-

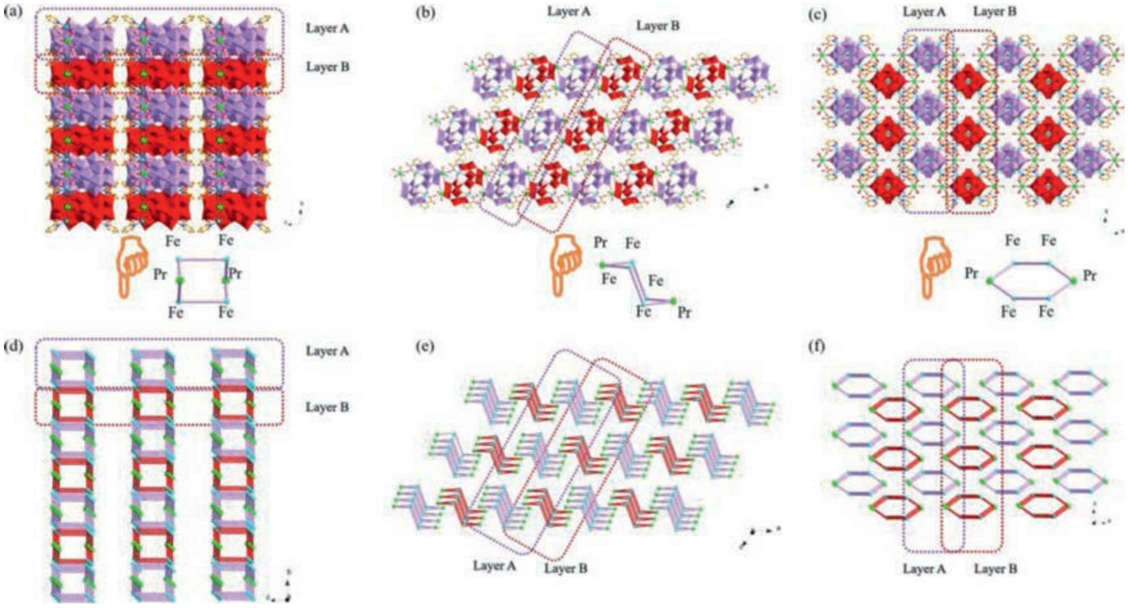

Fig. 2. (a–c) 3D stacking arrangements of anions of **1** viewed along *a*, *b* and *c* axes. (d–f) Simplified 3D stacking arrangements of anions of **1** viewed along *a*, *b* and *c* axes.

munosuppression, and increased risk of death. Therefore, develop the technique of monitoring trace NPP concentration is of great significance for the diagnosis and treatment of various neurological diseases [36–39]. In recent years, the determination methods of NPP mainly include fluorescent nanoprobes, enzyme biosensors and electrochemical sensors [40,41]. Electrochemical sensors toward NPP have been widely applied due to fast response speed, high detection efficiency, simple operation and low cost.

In fact, POM-based materials have been served as candidates for electrode materials because of their good electron exchange activity and redox ability [42–44]. Considering that the prepared crystalline material of **1** is difficult to dissolve in solvents under hydrothermal conditions, it can be mixed with carbon material to prepare **1**-CPE. It is shown that CPE prepared by graphite powder have better sensitivity and detection limit than carbon black or acetylene black [45]. Therefore, in this paper, graphite powder (60 mg), **1** (20 mg) and liquid paraffin wax (50 µL) are mixed and ground evenly, and filled in the electrode to produce the **1**-CPE electrochemical sensor to detect NPP. Before the electrochemically detecting NPP, the experiments to justify the stability of **1** in PBS were performed. Because **1** is insoluble in water, the crystals of **1** were immersed in PBS for 4 h and then the crystals were characterized by IR the spectrum (Fig. S2b in Supporting information). The IR spectra of **1** before and after immersing in PBS are almost the same, which illustrates the stability of **1** in PBS. First, CPE and **1**-CPE were placed in the 0.10 mol/L NaH_2PO_4–Na_2HPO_4 buffer solution (PBS) (pH 6.50) for cyclic voltammetry (CV) measurement (Fig. S3 in Supporting information). Compared with the CPE, **1**-CPE generates new oxidation peaks at +0.21 V and −0.18 V, among which the peak at +0.21 could be related to the redox process of Fe(III)/Fe(II) in **1**, while the peak at −0.18 V may be attributed to the redox process of W(VI)/W(IV) centers [46,47]. After that, CV curves of CPE and **1**-CPE were measured in the PBS containing 1.00 mmol/L NPP (Fig. 3a). At this time, a strong oxidation peak appears at +0.52 V and a corresponding reduction peak appears at −0.34 V, which was due to the redox reaction of NPP. Meanwhile, the peak intensity measured by **1**-CPE is much higher than that of CPE. Overall, it is indicated that the signal enhancement effect of **1** in **1**-CPE is quite significant.

In order to examine the stability of **1**-CPE, the CV method was used by 40 cycles in PBS (pH 6.50) containing 1.00 mmol/L NPP at a scan rate of 100 mV/s (Fig. S4 in Supporting information). As can be seen that the peak current value changes very little (Fig. 3b). Similarly, almost every curve is overlapped together in CV chart, and the change of the peak potential is very small, indicating that the stability of **1**-CPE is good, which can meet the following experimental requirements.

In addition, the relationship between scan rate (ν) and peak current is explored. The peak current generated by **1**-CPE in the PBS (pH 6.50) containing NPP at different scan rates of 20-100 mV/s was still tested. It can be seen from Fig. 3c that the oxidation peak potential becomes more positive with increasing scan rate, while the reduction peak potentials become more negative. Similarly, the peak current also changes regularly with the increase of scan rate: when the scan rate varies between 20 mV/s to 100 mV/s, the peak current (I_{pc}) is proportional to their square root, and the linear equation is I_{pc} (µA) = $2.29\nu^{1/2}$ $(mV/s)^{1/2}$ + 3.66, which reveals that the redox process of **1**-CPE is diffusion-controlled (Fig. 3d) [48].

Based on the requirement for detecting the NPP concentration, we explored the relationship between the NPP concentration and the peak current by the CV method. As the NPP concentration increases from 5 µmol/L to 1000 µmol/L, the peak current also gradually increases, and there is a linear relationship between them: I_{pc} (µA) = 0.016*c* (µmol/L) + 2.363 (Figs. 3e and f). The limit of determination (LOD) for **1**-CPE is calculated as 3.25 µmol/L on the base of three times the standard deviation of the blank sample. The low LOD and good linear relationship indicate the possibility for the efficient and rapid detection of the NPP concentration.

In order to further estimate the applicability of the **1**-CPE, the reproducibility and antijamming capability were tested. On one hand, in the process of detecting biological small molecules, there are usually interferences from other small molecules. To this end, 1.00 mmol/L arginine (ARG), alanine (ALA), tryptophan (TRP) and isoleucine (ILE) were separately added in the PBS (pH 6.50) containing 1.00 mmol/L NPP to observe its antijamming ability. It can be concluded from the coincidence degree of curves measured by CV and the histogram of peak current that **1**-CPE has good specificity detection capability (Fig. 4a and Fig. S5 in Supporting information). On the other hand, five electrodes were prepared and detected under the same conditions, and the relative standard deviation of peak current is 2.02%, which hints that **1**-CPE electrochemi-

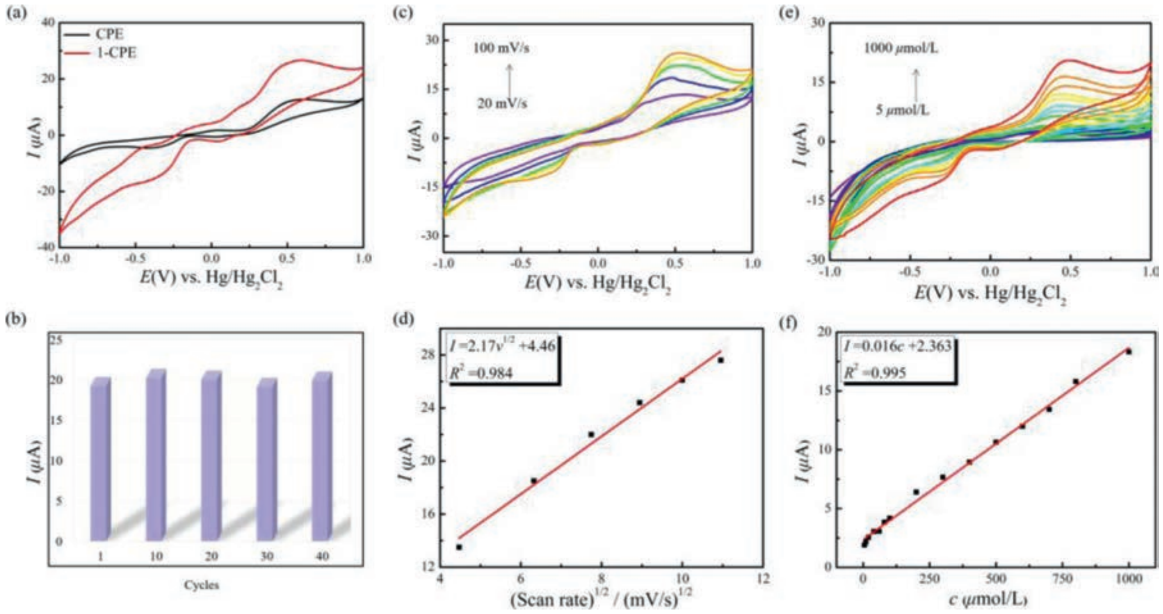

Fig. 3. (a) CV curves of CPE and **1**-CPE in the PBS (pH 6.50) containing 1.00 mmol/L NPP. (b) Comparison of current peak values at different scan cycles. (c) CV curves of **1**-CPE at different scan rate (20–100 mV/s) in the PBS (pH 6.50) containing 1.00 mmol/L NPP. (d) The linear equation between the peak current and the square root of scan rate. (e) CV curves of **1**-CPE in the PBS (pH 6.50) containing different concentrations of NPP (5–1000 μmol/L). (f) The linear equation between the peak current and the concentration of NPP.

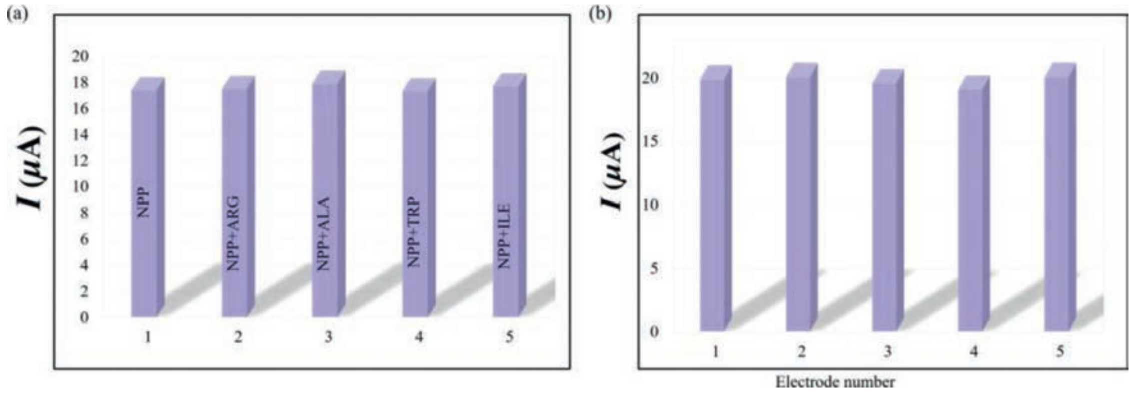

Fig. 4. (a) Comparison of the NPP peak current intensity measured in the presence of 1.00 mmol/L of different interferences (Alg, Ala, Trp, Ile). (b) Comparison of the peak current of the CV curve measured by five independent **1**-CPE ECSs in the PBS (pH 6.50) containing 1.00 mmol/L NPP.

cal sensors have considerable reproducibility (Fig. 4b and Fig. S6 in Supporting information). To date, there are few reports on POM-based material to electrochemically detect NPP. The electrochemically detecting performances of **1**-CPE towards NPP are comparable to those previously reported results [49–51].

In conclusion, we have hydrothermally synthetized and structurally characterized one pca-modified TRIG **1**, whose hybrid anion shows an unusual assembly constructed from an unusual *S*-type $[Ge_2W_{20}O_{72}]^{16-}$ cluster functionalized by four $[Fe(H_2O)(pca)]^{2+}$ and two terminal $[Pr(H_2O)_8]^{3+}$ groups. In addition, the electrochemical behaviors of **1** involving the detection toward NPP have been studied in the PBS, presenting potential applications in detection biomolecules. In the work, we can find that some unusual GT fragments can be continuously discovered by controlling appropriate hydrothermal reaction conditions. Moreover, the introduction and utilization of *N*-heterocyclic carboxylic acid ligands to the TM-RE-POM system is beneficial to construct and tune the structural diversity of TRIPs. In the future, others *N*-heterocyclic organic ligands and other different valent TMs will be introduced in the system to generate diverse TRIGs with novel structures and outstanding functional properties.

Declaration of competing interest

The authors declare no competing interest.

Acknowledgments

This work was supported by the National Natural Science Foundation of China (Nos. 21871077, 21671054, 21771052, 22071042), and the Program for Innovation Teams in Science and Technology in Universities of Henan Province (No. 20IRTSTHN004).

Supplementary materials

Supplementary material associated with this article can be found, in the online version, at doi:10.1016/j.cclet.2021.09.078.

References

[1] J.T. Rhule, C.L. Hill, D.A. Judd, et al., Chem. Rev. 98 (1998) 327–358.
[2] D.Y. Fu, S.M. Zhang, Z.Y. Qu, et al., ACS Appl. Mater. Interfaces 10 (2018) 6137–6145.
[3] J.C. Liu, Q. Han, L.J. Chen, et al., Angew. Chem. Int. Ed. 57 (2018) 8416–8420.
[4] K. Yang, Y. Hu, L. Li, et al., Nano Energy 74 (2020) 104851.

[5] S.J. Folkman, R.G. Finke, ACS Catal. 7 (2017) 7–16.
[6] X. Xu, X. Liu, D. Wang, et al., Inorg. Chem. 60 (2021) 1037–1044.
[7] J.Q. Sha, P.P. Zhu, X.Y. Yang, et al., Inorg. Chem. 56 (2017) 11998–12002.
[8] J.W. Zhang, Y.C. Huang, G. Li, et al., Coord. Chem. Rev. 378 (2019) 395–414.
[9] G.P. Yang, Y.F. Liu, K. Li, et al., Chin. Chem. Lett. 31 (2020) 3233–3236.
[10] H. Bian, X.J. Zhang, H.K. Zhao, et al., Chin. Chem. Lett. 30 (2019) 1097–1099.
[11] Y.W. Peng, C.S. Shan, H.J. Wang, et al., Adv. Energy Mater. 9 (2019) 1900597.
[12] H.Y. Zhao, Y.Z. Li, J.W. Zhao, et al., Coord. Chem. Rev. 440 (2021) 213966.
[13] X. Ma, W. Yang, L. Chen, et al., CrystEngComm 17 (2015) 8175–8197.
[14] J.C. Liu, J.F. Wang, Q. Han, et al., Angew. Chem. Int. Ed. 60 (2021) 11153–11157.
[15] S.T. Zheng, G.Y. Yang, Chem. Soc. Rev. 41 (2012) 7623–7646.
[16] X. Ma, H. Li, L. Chen, et al., Dalton Trans. 45 (2016) 4935–4960.
[17] P.T. Ma, F. Hu, J.P. Wang, et al., Coord. Chem. Rev. 378 (2019) 281–309.
[18] L.Z. Qiao, M. Song, A.F. Geng, et al., Chin. Chem. Lett. 30 (2019) 1273–1276.
[19] N. Zhang, L.Y. Hong, A.F. Geng, et al., Chin. Chem. Lett. 29 (2018) 1409–1412.
[20] Y. Hao, L. Zhong, H.H. Li, et al., Cryst. Growth Des. 19 (2019) 1329–1335.
[21] M. Samaniyan, M. Mirzaei, R. Khajavian, et al., ACS Catal. 9 (2019) 10174–10191.
[22] C. Boskovic, Acc. Chem. Res. 50 (2017) 2205–2214.
[23] V. Das, R. Kaushik, F. Hussain, Coord. Chem. Rev. 413 (2020) 213271.
[24] J.W. Zhao, Y.Z. Li, L.J. Chen, et al., Chem. Commun. 52 (2016) 4418–4445.
[25] Z.M. Zhang, Y.G. Li, S. Yao, et al., Dalton Trans. 40 (2011) 6475–6479.
[26] C.T. Kresge, M.E. Leonowicz, W.J. Roth, et al., Nature 359 (1992) 710–712.
[27] U. Kortz, S. Nellutla, A.C. Stowe, et al., Inorg. Chem. 43 (2004) 2308–2317.
[28] Y.Z. Li, J. Luo, L.J. Chen, et al., RSC Adv. 4 (2014) 50679–50692.
[29] S. Reinoso, J.R. Galán-Mascarós, Inorg. Chem. 49 (2010) 377–379.
[30] H.Y. Zhao, J.W. Zhao, B.F. Yang, et al., Cryst. Growth Des. 13 (2013) 5169–5174.
[31] J. Wang, J.W. Zhao, H.Y. Zhao, et al., CrystEngComm 16 (2014) 252–259.
[32] L. Zhong, X.X. Li, T. Yang, et al., Angew. Chem. Int. Ed. 56 (2017) 2664–2669.
[33] J.W. Zhao, D.Y. Shi, L.J. Chen, et al., Dalton Trans. 41 (2012) 10740–10751.
[34] J.W. Zhao, D.Y. Shi, L.J. Chen, et al., Cryst. Growth Des. 13 (2013) 4368–4377.
[35] J.W. Zhao, Y.Z. Li, F. Ji, et al., Dalton Trans. 43 (2014) 5694–5706.
[36] K.J. Samdani, D.W. Joh, M.K. Rath, et al., Electrochim. Acta 252 (2017) 268–274.
[37] F.M. Morawski, B.B. Xavier, A.H. Virgili, et al., Mater. Sci. Eng. C: Mater. Biol. Appl. 120 (2021) 111646–111657.
[38] M.Y. Emran, M. Mekawy, N. Akhtar, et al., Biosens. Bioelectron. 100 (2018) 122–131.
[39] J. Mårtensson, A.C. Gordon, Anal. Chim. Acta 1039 (2018) 124–131.
[40] T. Pradhan, H.S. Jung, J.H. Jang, et al., Chem. Soc. Rev. 43 (2014) 4684–4713.
[41] T. Chen, Y.H. Xu, S. Wei, et al., Biosens. Bioelectron. 124-125 (2019) 224–232.
[42] C.L. Zhou, S. Li, W. Zhu, et al., Electrochim. Acta 113 (2013) 454–463.
[43] J. Jiang, L.L. Liu, G.P. Liu, et al., Inorg. Chem. 59 (2020) 15355–15364.
[44] L.L. Liu, J. Jiang, X.Y. Liu, et al., Inorg. Chem. Front. 7 (2020) 4640–4651.
[45] A.A. Lahcen, S.A. Errayess, A. Amine, Microchim. Acta 183 (2016) 2169–2176.
[46] M. Sadakane, E. Steckhan, Chem. Rev. 98 (1998) 219–237.
[47] U. Kortz, M.G. Savelieff, B.S. Bassil, et al., Inorg. Chem. 41 (2002) 783–789.
[48] Z.G. Han, Y.L. Zhao, J. Peng, et al., Electrochim. Acta 51 (2005) 218–224.
[49] C.M. Kuskur, B.E. Kumara Swamy, H. Jayadevappa, Ionics (Kiel) 25 (2019) 1845–1855.
[50] B.N. Chandrashekar, B.E. Kumara Swamy, Anal. Methods 4 (2012) 849–854.
[51] H. Beitollahi, A. Mohadesi, S.K. Mahani, et al., Ionics (Kiel) 18 (2012) 703–710.